238

Copy
RM L53F18

NACA RM L53F18

7440

NACA

RESEARCH MEMORANDUM

FREE-FLIGHT LONGITUDINAL-STABILITY

INVESTIGATION INCLUDING SOME EFFECTS OF WING ELASTICITY

FROM MACH NUMBERS OF 0.85 TO 1.34 OF A TAILLESS MISSILE

CONFIGURATION HAVING A 45° SWEPTBACK

WING OF ASPECT RATIO 5.5

By Richard G. Arbic and Warren Gillespie, Jr.

Langley Aeronautical Laboratory
Langley Field, Va.

NATIONAL ADVISORY COMMITTEE
FOR AERONAUTICS

WASHINGTON
August 10, 1953

RECEIPT SIGNATURE
REQUIRED

NATIONAL ADVISORY COMMITTEE FOR AERONAUTICS

RESEARCH MEMORANDUM

FREE-FLIGHT LONGITUDINAL-STABILITY

INVESTIGATION INCLUDING SOME EFFECTS OF WING ELASTICITY

FROM MACH NUMBERS OF 0.85 TO 1.34 OF A TAILLESS MISSILE

CONFIGURATION HAVING A 45° SWEPTBACK

WING OF ASPECT RATIO 5.5

By Richard G. Arbic and Warren Gillespie, Jr.

SUMMARY

A free-flight longitudinal-stability investigation has been conducted between Mach numbers 0.85 and 1.34 to obtain the aerodynamic characteristics of a long-range, jet-propelled, ground-to-ground missile having a wing of aspect ratio 5.5, 45° sweepback, and taper ratio 0.4 mounted on a body with a vertical tail but no horizontal tail. Two models were flown, one with a wing of steel and the other with a wing of 75S-T6 aluminum alloy, to permit determination of aeroelastic effects on the lift-curve slope and aerodynamic center. Periodic pulse rocket disturbances in pitch permitted obtaining the longitudinal stability characteristics in addition to zero-lift drag and trim.

Analysis of data pertaining to longitudinal stability indicated the following: Wing flexibility reduced the lift-curve slope and shifted the aerodynamic center forward. The lift-curve slope was a maximum at Mach number 0.95 and had a value of 0.102 at this Mach number when corrected to the rigid-wing condition. Aerodynamic center corrected to the rigid-wing condition moved rearward from 27 percent mean aerodynamic chord at Mach number 0.9 to 46 percent at Mach number 1.1. Pitch damping decreased severely near Mach number 1 but had no large effect on the total damping.

INTRODUCTION

Tests have been conducted by the Langley Pilotless Aircraft Research Division to evaluate the transonic aerodynamic characteristics of a long-range, jet-propelled, ground-to-ground missile designed to cruise at high subsonic Mach numbers and to attain supersonic Mach numbers during the

terminal approach to the target. The missile has a wing and vertical tail mounted on a body of fineness ratio 13.94, but has no horizontal tail. Longitudinal control surfaces are on the wing. The wing has 45° sweepback, an aspect ratio of 5.5, and a taper ratio of 0.4. The airfoil section is 6 percent thick streamwise, and is slightly drooped at the leading edge.

The testing program was designed to yield the longitudinal stability characteristics of the missile with controls fixed and undeflected. Some effects of wing flexibility on the longitudinal stability were determined by flying two models, one with a wing of steel and the other with a wing of 75S-T6 aluminum alloy.

This paper presents the longitudinal stability, zero-lift drag, and longitudinal trim characteristics of the missile configuration as obtained from two free-flight rocket-powered models. The results are compared with those from a wind-tunnel test of the configuration presented in reference 1.

SYMBOLS

a_l longitudinal acceleration, positive forward, ft/sec^2

a_n normal acceleration, ft/sec^2

b wing span, ft

c local wing chord, ft

$\bar{c}$ wing mean aerodynamic chord, 0.82 ft

C_c chord-force coefficient, $-\dfrac{Wa_l}{gqS}$

C_D drag coefficient, $C_c \cos \alpha + C_N \sin \alpha$

C_L lift coefficient, $C_N \cos \alpha - C_c \sin \alpha$

C_{L_α} lift-curve slope per degree, $\dfrac{\partial C_L}{\partial \alpha}$

$C_{L_{\alpha_e}}$ elastic-wing lift-curve slope per degree

$C_{L_{\alpha_r}}$ rigid-wing lift-curve slope per degree

C_m　　pitching-moment coefficient,

$$\frac{\text{Pitching moment about center of gravity}}{qS\bar{c}}$$

C_{m_α}　　pitching-moment-curve slope per degree, $\dfrac{\partial C_m}{\partial \alpha}$

C_N　　normal-force coefficient, $\dfrac{Wa_n}{gqS}$

C_{n_β}　　yawing-moment-curve slope per degree, $\dfrac{\partial C_n}{\partial \beta}$

g　　acceleration due to gravity, 32.2 ft/sec^2

I_Y　　moment of inertia in pitch about center of gravity

I_Z　　moment of inertia in yaw about center of gravity

L　　applied load, lb

M　　Mach number

P　　period, sec

q　　dynamic pressure, lb/ft^2

R　　Reynolds number based on wing mean aerodynamic chord

S　　total wing area including portion in fuselage, 3.27 ft^2

t　　wing airfoil thickness, ft

$T_{1/2}$　　time for oscillation to damp to one-half amplitude, sec

V　　velocity, ft/sec

W　　weight, lb

y　　distance to any spanwise station from fuselage center line, ft

$\dfrac{y}{b/2}$　　nondimensional spanwise station parameter

α　　angle of attack, deg

$\dot{\alpha}$　　$\dfrac{1}{57.3}\dfrac{d\alpha}{dt}$, radians/sec

θ local wing twist angle produced by L, deg; also angle of pitch, deg

$\dot{\theta}$ $\dfrac{1}{57.3}\dfrac{d\theta}{dt}$, radians/sec

ρ air density, slugs/ft^3

$\left(\dfrac{\theta}{L}\right)_{ref}$ structural influence coefficient at spanwise center of pressure

The pitch-damping derivatives are expressed as follows:

$$\left(C_m\right)_{\frac{\dot{\theta}\bar{c}}{2V}} = \frac{\partial C_m}{\partial\frac{\dot{\theta}\bar{c}}{2V}} \qquad \left(C_m\right)_{\frac{\dot{\alpha}\bar{c}}{2V}} = \frac{\partial C_m}{\partial\frac{\dot{\alpha}\bar{c}}{2V}}$$

MODELS AND INSTRUMENTATION

The two models tested were of metal construction and were identical except for wing material. One model had a wing of solid 75S-T6 aluminum alloy and the other a steel wing plated with a layer of cadmium alloy for ease of machining. The cadmium-steel wing had a modulus of elasticity 2.15 times that of the dural wing. For simplicity, the 75S-T6 wing will hereafter be referred to as the dural wing and the cadmium-steel wing as the steel wing.

The wings had an aspect ratio of 5.5, taper ratio 0.4, and 45° sweepback of the 0.406 streamwise chord line. The airfoil section was approximately 6 percent thick streamwise and was slightly drooped at the leading edge. The wing was set at 0° incidence with respect to the fuselage center line. For the models of the present test, the body had a fineness ratio of 13.94, whereas the wind-tunnel model of reference 1 had a body fineness ratio of 12.9. The higher fineness ratio body was obtained by lengthening the nose. The missile configuration has no horizontal tail but has a vertical tail swept back 33° at the 40-percent-chord line.

A three-view drawing of the models is shown in figure 1 and photographs are presented as figure 2. The method of launching and boosting the models is shown in figure 3. Table I gives the wing, body, and vertical-tail ordinates and shows a sketch of the drooped-leading-edge airfoil section. Table II gives the dimensional and mass characteristics.

The models were equipped with pulse rockets located in the cylindrical portion of the body rearward of the wing. These pulse rockets disturbed the models in pitch.

Model instrumentation consisted of a total-pressure probe mounted on a strut beneath the body, an angle-of-attack indicator mounted on a

boom ahead of the body, two normal accelerometers, a longitudinal accel-
erometer, and a transverse accelerometer. A six-channel telemeter located
in the nose was used to transmit quantities measured by the instruments.

TESTS

The dural and steel wings were static tested to obtain structural
influence coefficients by application of loads at five spanwise stations
along the 25-percent-streamwise-chord line for the dural wing and along
the 25- and 40-percent-chord lines for the steel wing.

The models were boosted to maximum velocity by an ABL Deacon rocket
motor. After drag-inertia separation, the models decelerated through the
Mach number range while experiencing short-period oscillations following
the disturbances from the pulse rockets. A telemeter ground station
recorded the six continuous channels of information. Model velocity was
obtained by use of the CW Doppler radar unit and was corrected for the
effect of winds at altitude and for flight-path curvature. An NACA modi-
fied SCR 584 radar tracking unit was used to obtain model trajectory data.
Free-stream temperature and static pressure, and the wind velocity at
altitude were obtained from a radiosonde balloon tracked by the 584 radar
unit.

Reynolds number and dynamic pressure of the tests are shown as a
function of Mach number in figure 4. For comparison, Reynolds number and
dynamic pressure for the smaller wind-tunnel model of reference 1 are also
presented. For the present tests, Reynolds number, based on the model
wing mean aerodynamic chord of 0.82 foot, varied from approximately
3.5×10^6 to 7×10^6, and the dynamic pressure range was approximately
750 to 2,300 pounds per square foot.

The dural and steel wing models were flown with respective center-
of-gravity locations of 78.8- and 31.5-percent mean aerodynamic chord
forward of the leading edge of the mean aerodynamic chord.

Flight tests were conducted at the Pilotless Aircraft Research
Station, Wallops Island, Va.

ANALYSIS

Time histories of the coasting portion of flight following separation
of the model from the booster were analyzed to obtain lift, zero-lift drag,
and static stability characteristics for each model. Separation from the

booster and the periodic firing of the pulse rockets produced pitching oscillations at intervals along the flight path permitting analysis of both trimmed flight and pitching flight.

Trimmed Flight

The zero-lift drag coefficient was calculated by two independent methods. One method made use of accelerations obtained by differentiation of the Doppler determined velocity-time curve. The second method made use of chord-force measurements from the longitudinal accelerometer since the models trimmed at virtually zero normal force. In a similar manner, trim normal-force coefficient was obtained from measurements by the normal accelerometers. Trim angle of attack was read directly from the telemeter trace of angle of attack.

Pitching Flight

The angles of attack measured while the model was pitching were corrected for flight-path curvature and rate of pitch about the model center of gravity as described in reference 2. Lift coefficient was determined by transferring the normal- and chord-force coefficients measured at the model center of gravity to the stability axes. The lift-curve slope was then obtained from plots of lift coefficient against angle of attack using the three highest amplitude cycles of the oscillation produced by each disturbance. The lift-curve slope determined from each of these cycles of the oscillation was then plotted against the average Mach number for the cycle.

The total damping was obtained from the envelope of the decaying oscillations and the sum of the pitch-damping derivatives $(C_m)_{\dot{\theta}\bar{c} \over 2V}$ and $(C_m)_{\dot{\alpha}\bar{c} \over 2V}$ was determined from the expression:

$$(C_m)_{\dot{\theta}\bar{c} \over 2V} + (C_m)_{\dot{\alpha}\bar{c} \over 2V} = - \frac{8I_Y}{\rho V S \bar{c}^2} \left(\frac{0.693}{T_{1/2}} - \frac{57.3 C_{L_\alpha} \rho V S g}{4W} \right)$$

Static longitudinal stability was obtained from a relation between model moment of inertia in pitch and the periods and damping of the oscillations. The relationship can be written as follows:

$$C_{m_\alpha} = - \frac{I_Y}{57.3 q S \bar{c}} \left(\frac{4\pi^2}{P^2} + \frac{0.480}{T_{1/2}^2} \right)$$

From low-amplitude lateral oscillations induced when the models pitched, the yawing-moment coefficient due to sideslip C_{n_β} was obtained from the relationship:

$$C_{n_\beta} \approx \frac{4\pi^2 I_Z}{57.3 q S b P^2}$$

This expression is approximate in that it does not include damping, but the damping term is small and contributes little to the value of C_{n_β}.

A more detailed description of the method of analysis and general limitations of the pulse technique is presented in reference 3.

Aeroelastic Calculations

Aeroelastic calculations to obtain the lift-curve slope and center of pressure for a model with a rigid wing were made by assuming a span load distribution from the theoretical charts of reference 4 and calculating the ratio of elastic to rigid lift-curve slope and incremental static stability as described in the appendix of reference 5. The method used herein differed from the method of reference 5 in that a six-point load distribution was assumed for the total half span rather than a five-point distribution for the exposed half span. This was done to obtain the ratio of $\dfrac{C_{L_{\alpha e}}}{C_{L_{\alpha r}}}$ for the complete model since the wing-alone lift was not measured. Inertia loading effects were included in the calculations since these were found to be appreciable for the models of the present test.

ACCURACY

It is difficult to calculate the exact limits of accuracy of all the various quantities and coefficients obtained from free-flight models, since these are often determined from measurements of a combination of several instruments of varying degrees of accuracy and reliability. However, experience from tests of identical models and investigations of the reliability of the various instruments have resulted in accepted ranges of

accuracy. On this basis, the estimated maximum errors in some of the data for the models of the present tests are stated below:

	M = 0.9	M = 1.25
Mach number	±0.008	±0.005
Angle of attack, deg	±0.4	±0.4
Drag coefficient.	±0.001	±0.0007
Normal-force coefficient	±0.015	±0.004
Lift-curve slope	±0.0020	±0.001

RESULTS AND DISCUSSION

The experimental data obtained during coasting flight of the two models are presented in figures 5 to 10, and results of the aeroelastic calculations are presented in figures 11 to 13.

Trimmed Flight

Trim drag coefficient, normal-force coefficient, and angle of attack are presented as a function of Mach number in figure 5. The trim drag coefficient shown is essentially the zero-lift drag coefficient since the models trimmed to virtually zero normal force. From a subsonic value of 0.0127, the drag coefficient increases sharply between Mach numbers 0.95 and 1.1 and then more gradually to a maximum value of 0.0325 at Mach number 1.35. The drag coefficient from the wind-tunnel test of reference 1 is seen to be lower subsonically and slightly higher supersonically than that of the present test possibly due to basic differences in the models and test Reynolds numbers. The trim normal-force coefficient and trim angle of attack plotted as a function of Mach number show that the slightly drooped leading edge of the wing results in a positive angle of attack of approximately 0.6° subsonically and 0.85° supersonically for essentially zero normal-force coefficients of -0.004 and 0.004.

Pitching Flight

Lift.- Basic data curves of lift coefficient against angle of attack are presented in figure 6 for the dural and steel wing models at various Mach numbers. The variation of lift coefficient with angle of attack is linear for the range of lift coefficients covered.

Lift-curve and pitching-moment-curve slopes.- The effect of Mach number on the derivatives C_{L_α} and C_{m_α} is shown in figure 7. The maximum value of C_{L_α} occurs near a Mach number of 0.95. At Mach number 0.9 the

steel wing shows an increase of 17.7 percent in C_{L_α} over that of the more flexible dural wing, and at Mach number 1.25 the increase is 25.0 percent. These results compare favorably with the solid-steel wing wind-tunnel model of reference 1 at Mach numbers 0.85 and 0.92. For these Mach numbers the dynamic pressures of the test of reference 1 are comparable to those of the present test (see fig. 4). At the higher Mach numbers of 1.3 and 1.4 the wind-tunnel dynamic pressures were considerably lower than those of the present test and this probably accounts for the greater difference in C_{L_α} between the wind-tunnel test and the present test at the higher Mach numbers. Aeroelastic calculations (discussed more fully in a later section) indicate that for the dynamic pressures of the present test a rigid-wing configuration should have lift-curve-slope increases over the steel wing model of 13.8 percent at Mach number 0.9 and 23.1 percent at Mach number 1.25. The corresponding increases over the dural wing model are approximately 34.0 and 53.8 percent.

The pitching-moment derivative C_{m_α} in figure 7(b) is shown for the respective centers of gravity of the dural and steel wing models of 78.8 and 31.5 percent mean aerodynamic chord forward of the leading edge of the mean aerodynamic chord. The pitching-moment derivative is greatest near Mach number 1.0 and decreases gradually for lower and higher values of Mach number. Increasing wing flexibility results in decreased static stability with increasing Mach number and slightly lowers the Mach number for maximum static stability.

Longitudinal period and aerodynamic center.- The variations with Mach number of the period of the longitudinal short-period oscillation and of the aerodynamic-center location are shown in figure 8. Periods for both models decrease uniformly with increasing Mach number and reach a minimum value near Mach number 1.3.

Aerodynamic-center location plotted as a function of Mach number in figure 8(b) shows that the aerodynamic center moves rearward between Mach numbers of 0.9 and 1.1 and then begins a gradual forward movement. The forward movement above Mach number 1.1 is more pronounced for the dural wing model. For this model the rearward movement of the aerodynamic center is from 11 to 27 percent of the mean aerodynamic chord, and the corresponding values for the steel wing model are from 22 to 37 percent. Aeroelastic calculations to obtain the aerodynamic center for a model with a rigid wing show a disagreement between test models of about 4 percent of the mean aerodynamic chord at Mach number 0.9 but are in good agreement at the higher Mach numbers. The rearward movement of the aerodynamic center for a rigid wing is from 27 to 46 percent. The aerodynamic center obtained from reference 1 is approximately 5 percent more rearward than these rigid-wing values. The reason for this difference is not known.

Longitudinal damping.- The time for the longitudinal oscillation to damp to one-half amplitude, and the sum of the pitch-damping deriva-tives $\left(C_m\right)_{\frac{\dot{\theta}\bar{c}}{2V}} + \left(C_m\right)_{\frac{\dot{\alpha}\bar{c}}{2V}}$ are presented in figure 9. The time to damp to one-half amplitude is less at supersonic Mach numbers than at subsonic Mach numbers. This reduction continues at supersonic speeds for the dural wing model but shows a tendency to decrease for the steel wing model. The time to damp to one-half amplitude was less for the model with the dural wing, probably due primarily to a more-forward center-of-gravity location.

In figure 9(b) the sum of the pitch-damping derivatives is seen to decrease rapidly near Mach number 1 and, in fact, is positive in this region for the steel wing model which has the poorer damping character-istics throughout the Mach number range. The lower pitch-damping values for the steel wing model are thought to be due largely to the more rear-ward center-of-gravity location for this model and indicate that the practical flight range of center of gravity locations would produce even lower values of the pitch-damping coefficients. It is of interest to note, however, that the poor transonic pitch-damping characteristics have no large adverse effect on the total damping characteristics presented in figure 9(a). Above Mach number 1 the value of $\left(C_m\right)_{\frac{\dot{\theta}\bar{c}}{2V}} + \left(C_m\right)_{\frac{\dot{\alpha}\bar{c}}{2V}}$ increases to a nearly constant value for the dural wing model, but for the steel wing model rises to a peak near Mach number 1.1 and decreases for the higher Mach numbers. In view of this different trend for the pitch damping at the higher Mach numbers, the data were carefully reexamined to confirm the validity of the test points at respective Mach numbers of 1.33 and 1.25 for the dural and steel wing models, but no clue as to the reason for the different trends could be found.

Reference 6 presents a summary of the pitch-damping characteristics of several airplane and missile configurations as obtained from rocket-model tests. The swept-wing—body configuration of figure 3 in this reference is shown to have pitch-damping characteristics similar to that of the present-test configuration.

Lateral period and C_{n_β}.- The lateral period and C_{n_β} obtained from the induced low-amplitude lateral oscillations are presented in figure 10 as a function of Mach number for the respective center-of-gravity loca-tions of the models. The test points show considerable scatter due to the irregular nature of the oscillations. The period at Mach number 0.9 is approximately twice as long as at Mach number 1.3. Values for the yawing-moment coefficient due to sideslip C_{n_β} agree well with test

points at Mach numbers 0.85 and 1.4 from reference 1, corrected to the center-of-gravity location of the dural wing model. For the present test C_{n_β} should be lower than for the model of reference 1, due to a more flexible magnesium vertical tail on the flight model.

Aeroelastic Calculations

Results of the aeroelastic calculations, obtained in the manner described in reference 5, are presented in figures 11 to 13. Inertia loading effects were found to be appreciable for the models of the present tests and were, therefore, included in the calculations.

The structural influence coefficients obtained for the steel wing are presented in figure 11 as curves of θ/L against the spanwise station parameter $\frac{y}{b/2}$ for loads applied along the 25- and 40-percent-streamwise-chord lines.

Figure 12 presents two ways of extrapolating the test data to obtain rigid-wing values of C_{L_α}. The independent variable for these plots is the parameter $qS\left(\frac{\theta}{L}\right)_{ref}$ where $\left(\frac{\theta}{L}\right)_{ref}$ is the structural influence coefficient at the spanwise center of pressure of the rigid wing for a load applied at this spanwise location. Figure 12(a) shows a straight-line extrapolation of the test data for the two models of the present test. In figure 12(b) experimental data from the test of reference 1 were used in conjunction with data from the present test. Since inertia loading effects were not present in the wind-tunnel test, the lift-curve-slope data from the present test were put on a comparable basis by taking out the increment of C_{L_α} due to inertia loading. This incremental reduction of C_{L_α} is shown as the difference between the broken line and solid line symbols in figure 12(b) and was obtained from figure 13 which shows the effect of inertia loading on the calculated ratio $C_{L_{\alpha_e}}/C_{L_{\alpha_r}}$ plotted against the parameter $C_{L_{\alpha_r}}q$. The rigid-wing values of C_{L_α} obtained from the two methods of extrapolation are shown in figure 7(a). The ratio of the flexible C_{L_α} values to the extrapolated rigid values are shown in figure 13. These values agree with the calculated results for loads applied along the 0.25-chord line. This agreement of experimental and calculated data should indicate that the ratio $C_{L_{\alpha_e}}/C_{L_{\alpha_r}}$ thus obtained is of the correct order of magnitude. The ratio $C_{L_{\alpha_e}}/C_{L_{\alpha_r}}$ obtained

from figure 12(a) results in slightly higher experimental values than those from figure 12(b) due to a different value of $C_{L_{\alpha_r}}$ obtained for the two-point extrapolation. It is interesting to note, however, that these $C_{L_{\alpha_r}}$ values do not differ widely as evidenced by the plot of these points in figure 7(a). This is due to the steeper slope of the two-point straight-line extrapolation, arising largely from inertia loading effects of the heavier steel wing, the heavier wing changing the ratio of wing weight to model weight in such a manner as to produce the steeper straight-line slope. This fortunate circumstance often permits obtaining a reasonable value of $C_{L_{\alpha_r}}$ by a straight-line extrapolation of experimental data from two models having wings of different stiffnesses.

A test of the correctness of the extrapolated values of $C_{L_{\alpha_r}}$ may be obtained by calculating (as in fig. 13) the ratio $C_{L_{\alpha_e}}/C_{L_{\alpha_r}}$ from influence coefficients obtained for the wing and dividing the experimental values of $C_{L_{\alpha_e}}$ by this ratio for the various Mach numbers. If the curve of $C_{L_{\alpha_r}}$ is obtained in this manner for two or more wings of different stiffness, and these curves agree, the resulting values of $C_{L_{\alpha_r}}$ should be correct. The broken-line curves of figure 7(a) were obtained in the above manner for the two models of the present test and show good agreement together and with the extrapolated values of $C_{L_{\alpha_r}}$.

In figure 13, the data for the steel-wing model show that movement of the center of pressure from the 25- to the 40-percent-chord line results in an average decrease in $C_{L_{\alpha_e}}/C_{L_{\alpha_r}}$ of approximately 2 percent for the test range of $C_{L_{\alpha_r}}q$. The experimental points of $C_{L_{\alpha_e}}/C_{L_{\alpha_r}}$ from figure 12 should show better agreement with the calculated 40-percent-chord-line data than with the 25-percent-chord-line data at the higher values of $C_{L_{\alpha_r}}q$. The better agreement of the experimental points with the 25-percent-chord-line curve indicates some inaccuracies in the calculated and experimental data.

CONCLUSIONS

The results of free-flight rocket-model tests of two models of a swept-wing missile configuration indicated the following conclusions:

1. Due to wing flexibility, the lift-curve slope of the steel wing model was 17.7 percent higher than that of the dural wing model at a Mach number of 0.95, and 25 percent higher at Mach number 1.25.

2. Aeroelastic calculations and extrapolation of the test data indicated that a rigid-wing configuration should have lift-curve-slope increases over the steel wing model of 13.8 percent at Mach number 0.9 and 23.1 percent at Mach number 1.25 for the dynamic pressures of the test.

3. The maximum value of C_{L_α} occurred near a Mach number of 0.95. The lift-curve slope corrected to the rigid-wing condition increased uniformly from 0.088 at Mach number 0.85 to a maximum value of 0.102 and then decreased uniformly to 0.077 at Mach number 1.3.

4. Due to wing flexibility, the aerodynamic-center location for the steel wing was 10 percent mean aerodynamic chord farther rearward than that for the dural wing and approximately 6.5 percent farther forward than that for a rigid wing.

5. The aerodynamic center moved rearward between Mach numbers of 0.9 and 1.1 and then forward at higher Mach numbers. For a rigid wing the rearward movement would be from 27 to 46 percent.

6. The time to damp to one-half amplitude was less at supersonic Mach numbers than at subsonic Mach numbers. The sum of the pitch-damping derivatives decreased severely near Mach number 1 but had no large effect on the total damping.

Langley Aeronautical Laboratory,
    National Advisory Committee for Aeronautics,
        Langley Field, Va., June 9, 1953.

CONFIDENTIAL

REFERENCES

1. Phelps, E. Ray, and Lazzeroni, Frank A.: Wind-Tunnel Investigation
   of the Aerodynamic Characteristics of a 1/15-Scale Model of the
   Northrop MX-775A Missile. NACA RM A51E28, 1951.

2. Mitchell, Jesse L., and Peck, Robert F.: An NACA Vane-Type Angle of
   Attack Indicator for Use at Subsonic and Supersonic Speeds. NACA
   RM L9F28a, 1949.

3. Gillis, Clarence L., Peck, Robert F., and Vitale, A. James: Pre-
   liminary Results From a Free-Flight Investigation at Transonic and
   Supersonic Speeds of the Longitudinal Stability and Control Charac-
   teristics of an Airplane Configuration With a Thin Straight Wing of
   Aspect Ratio 3. NACA RM L9K25a, 1950.

4. DeYoung, John, and Harper, Charles W.: Theoretical Symmetric Span
   Loading at Subsonic Speeds for Wings Having Arbitrary Plan Form.
   NACA Rep. 921, 1948.

5. Vitale, A. James: Effects of Wing Elasticity on the Aerodynamic
   Characteristics of an Airplane Configuration Having 45° Sweptback
   Wings As Obtained From Free-Flight Rocket-Model Tests at Transonic
   Speeds. NACA RM L52L30, 1953.

6. Gillis, Clarence L., and Chapman, Rowe, Jr.: Summary of Pitch-Damping
   Derivatives of Complete Airplane and Missile Configurations As
   Measured in Flight at Transonic and Supersonic Speeds. NACA
   RM L52K20, 1953.

TABLE I

BODY, WING, AND VERTICAL-TAIL ORDINATES

Body ordinates		Wing ordinates, percent chord			Vertical-tail ordinates, percent chord	
Station, in. from nose	Radius, in.	Station	Upper surface	Lower surface	Station	Upper and lower surfaces
0	0	0	-0.850	0.850	0	0
1.4	.380	1.25	.200	1.573	1.25	.960
2.0	.548	2.50	.610	1.855	2.50	1.335
4.0	1.066	5.00	1.120	2.190	5.00	1.770
6.0	1.502	7.50	1.480	2.410	7.50	2.060
8.0	1.857	10.00	1.773	2.567	10.00	2.265
10.0	2.151	15.00	2.227	2.782	15.00	2.567
12.0	2.390	20.00	2.532	2.922	20.00	2.770
14.0	2.575	25.00	2.747	2.998	25.00	2.907
17.0	2.770	30.00	2.900	3.033	30.00	3.010
20.0	2.878	35.00	2.980	3.040	40.00	3.120
22.0	2.900	40.00	3.010	3.020	50.00	3.057
Straight line		50.00	2.855	2.860	60.00	2.810
65.0	2.900	60.00	2.380	2.380	70.00	2.395
68.0	2.875	70.00	1.812	1.812	75.00	2.090
70.0	2.810	80.00	1.233	1.233	Straight line	
72.0	2.700	90.00	.640	.640	100.00	.100
74.0	2.545	100.00	.015	.015		
76.0	2.340					
78.0	2.070					
80.0	1.710					
80.9	1.500					

$$\left(\frac{t}{c}\right)_{max} = 0.0603c$$
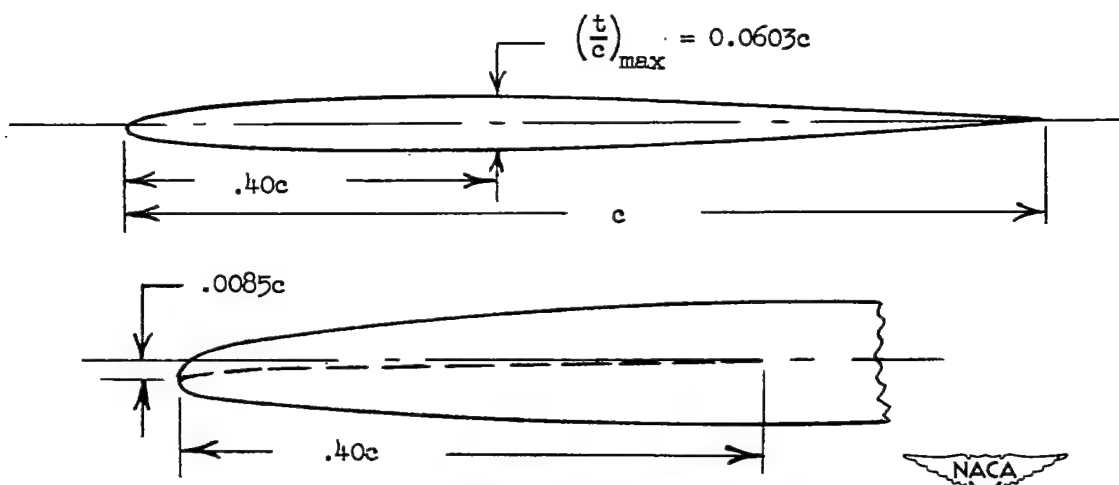
Wing airfoil section and leading edge droop detail.

TABLE II

PHYSICAL CHARACTERISTICS OF THE DURAL AND STEEL WING MODELS

	Dural wing model	Steel wing model
Wing:		
Area (total included), sq ft	3.27	3.27
Span, ft	4.23	4.23
Aspect ratio	5.5	5.5
Mean aerodynamic chord, ft	0.82	0.82
Sweepback of 0.4-chord line, deg	45	45
Dihedral (relative to mean thickness line), deg. .	0	0
Taper ratio, tip chord/root chord	0.4	0.4
Vertical tail:		
Area (extended to center line), sq ft	0.45	0.45
Height (above fuselage center line), ft	1	1
Sweepback of 0.4-chord line, deg	33	33
Taper ratio, tip chord/root chord	0.286	0.286
Fuselage:		
Length, ft	6.73	6.73
Maximum diameter, ft	0.483	0.483
Fuselage fineness ratio, length/diameter . . .	13.94	13.94
Nose fineness ratio	4.14	4.14
Boattail fineness ratio	2.76	2.76
Weight and balance:		
Weight, lb	88.7	111.8
Wing loading	27.1	34.1
Center-of-gravity position (percent $\bar{c}$ forward of leading edge of mean aerodynamic chord) . .	78.8	31.5
Moment of inertia in pitch, I_Y, slug-ft^2	8.90	8.51
Moment of inertia in yaw, I_Z, slug-ft^2	8.90	9.82
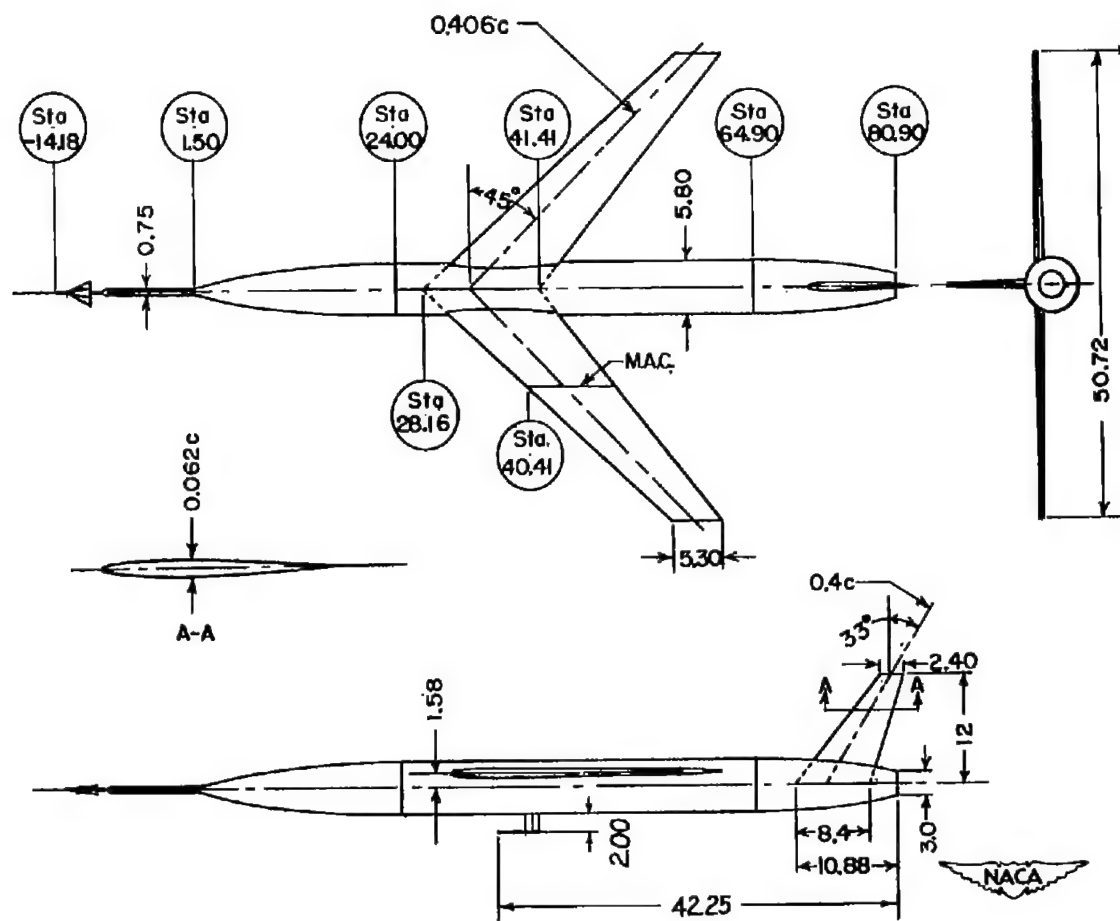
Figure 1.- General arrangement of test models. All dimensions are in inches.
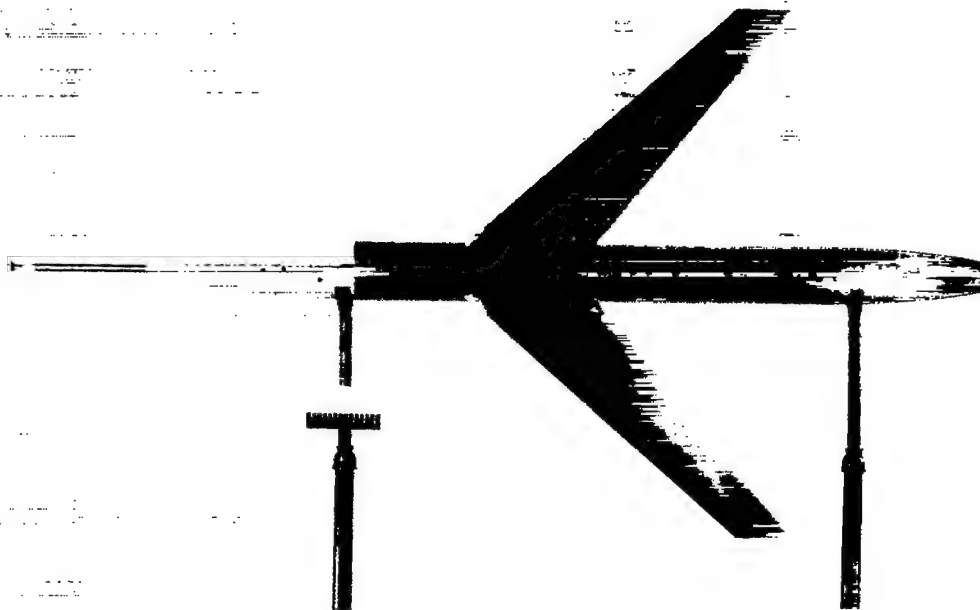
(a) Side view.
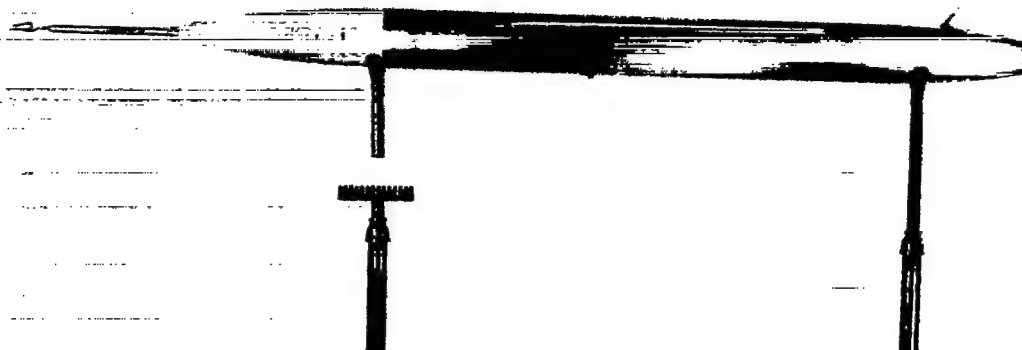
L-73202

(b) Top view.

Figure 2.- Photographs of model.

L-73201
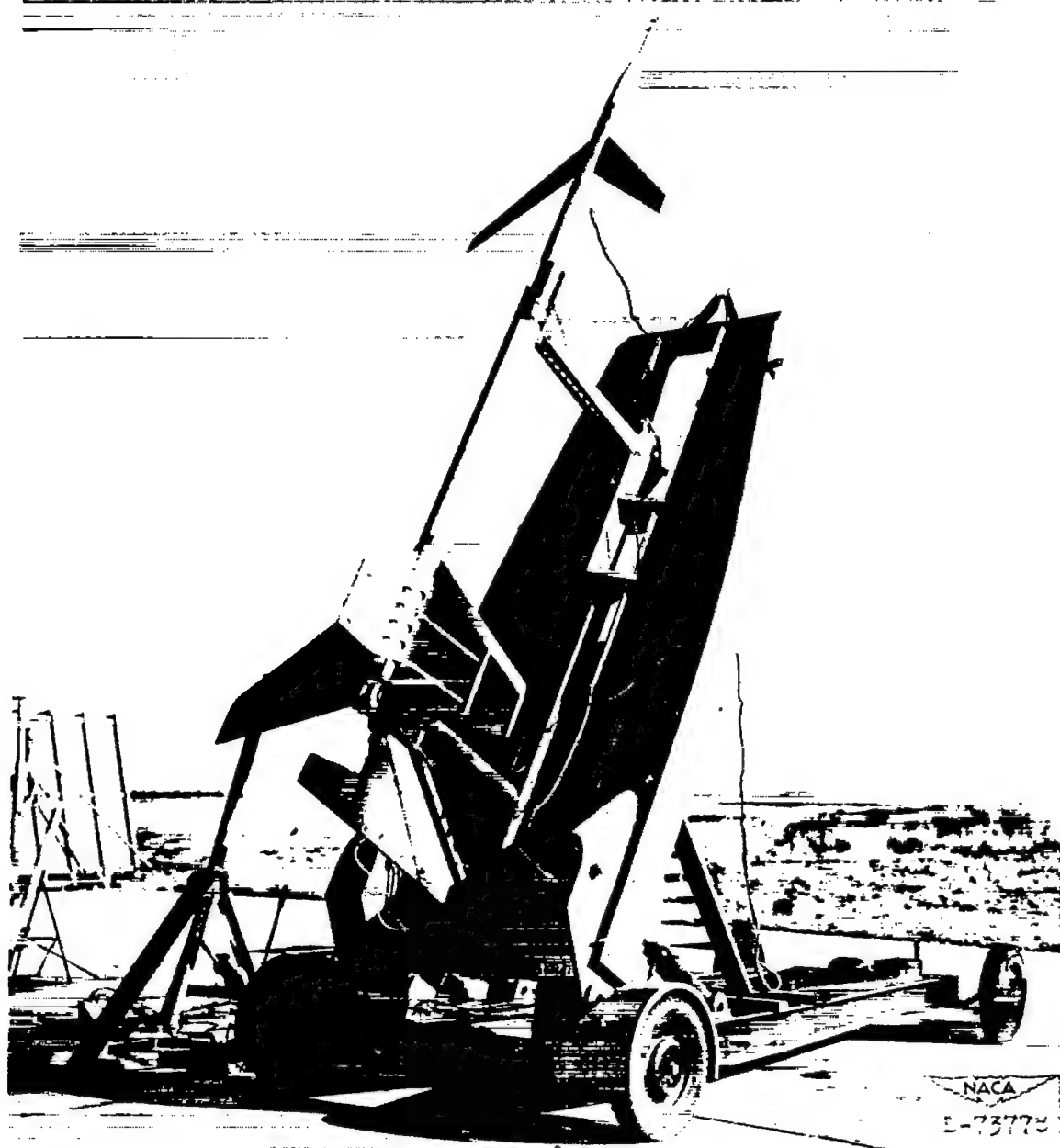
Figure 3.- Photograph of model and booster on launcher.
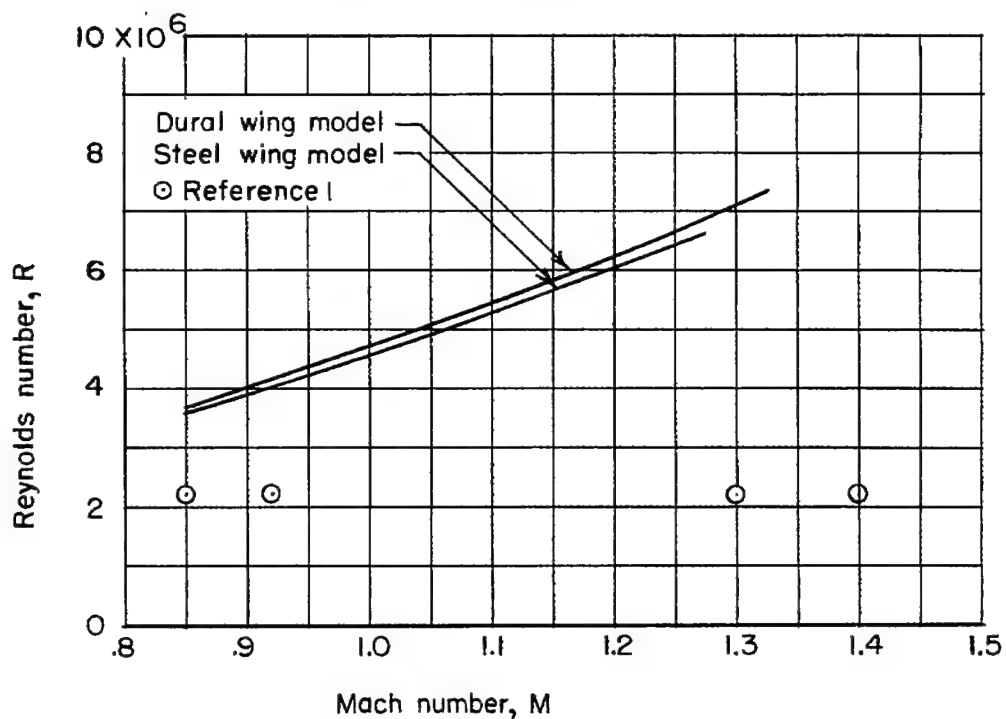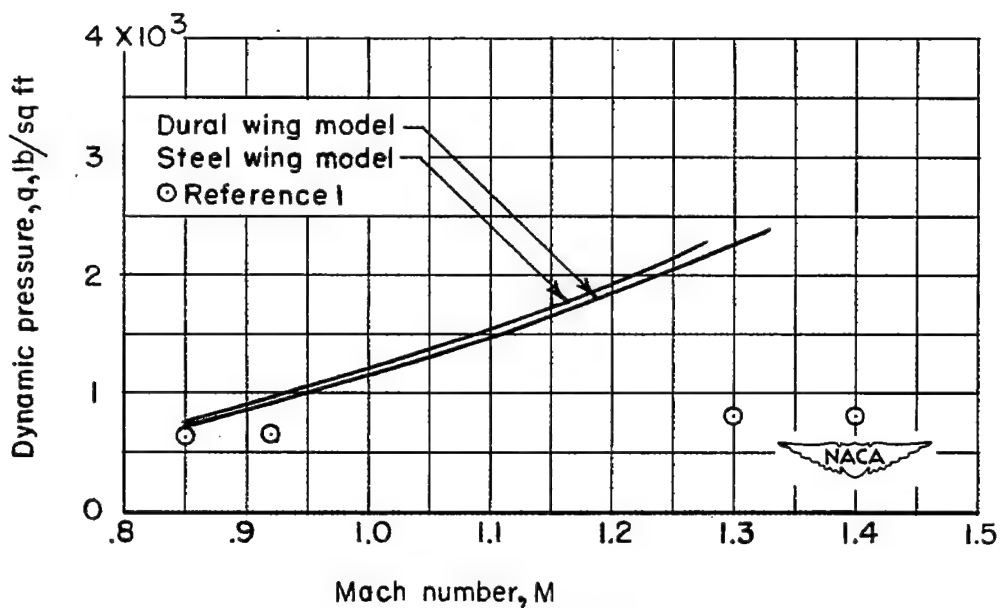
(a) Reynolds number.

(b) Dynamic pressure.

Figure 4.- Variation of Reynolds number and dynamic pressure with
Mach number.
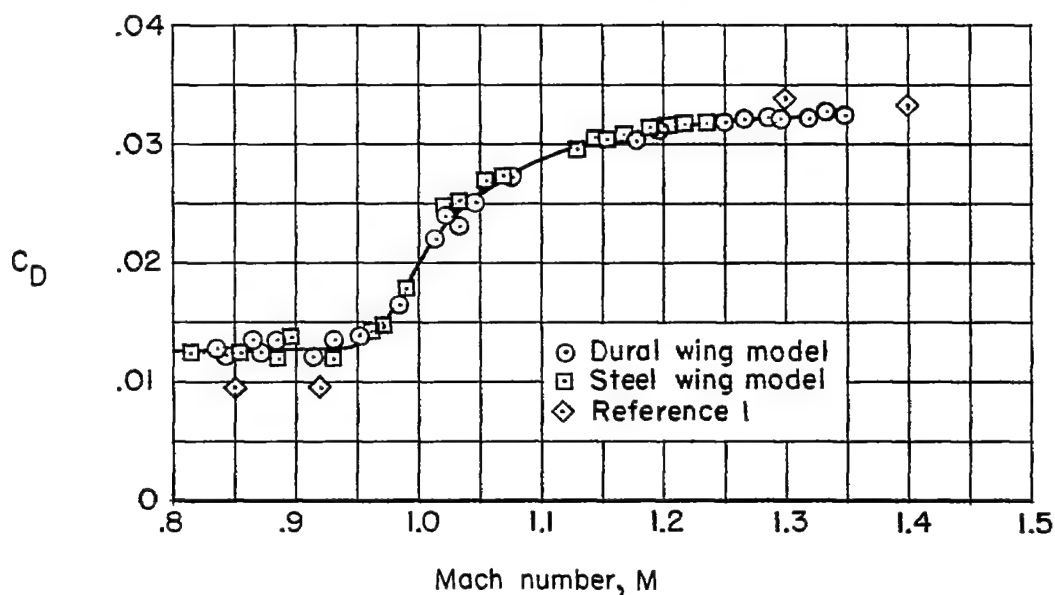
(a) Drag coefficient.
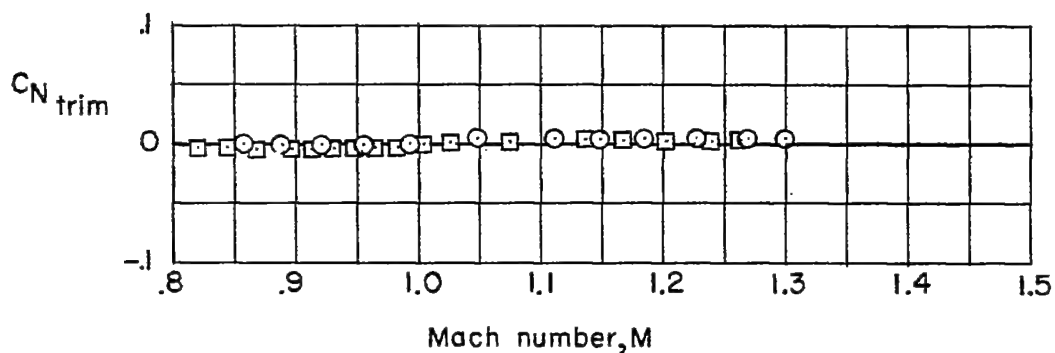
(b) Trim normal-force coefficient.
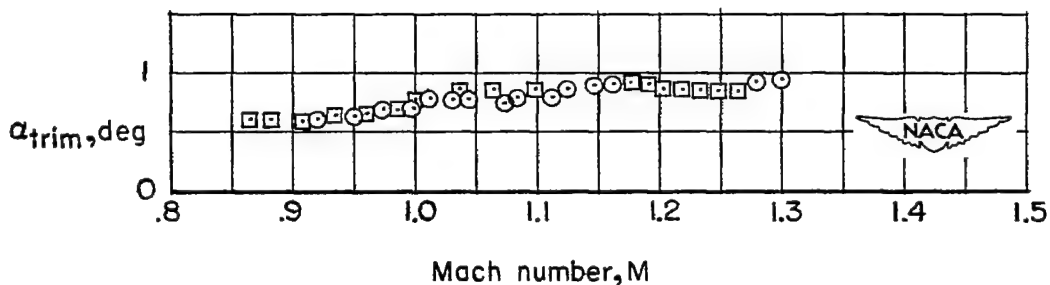
(c) Trim angle of attack.

Figure 5.- Effect of Mach number on the zero-lift drag coefficient, trim
normal-force coefficient, and trim angle of attack.
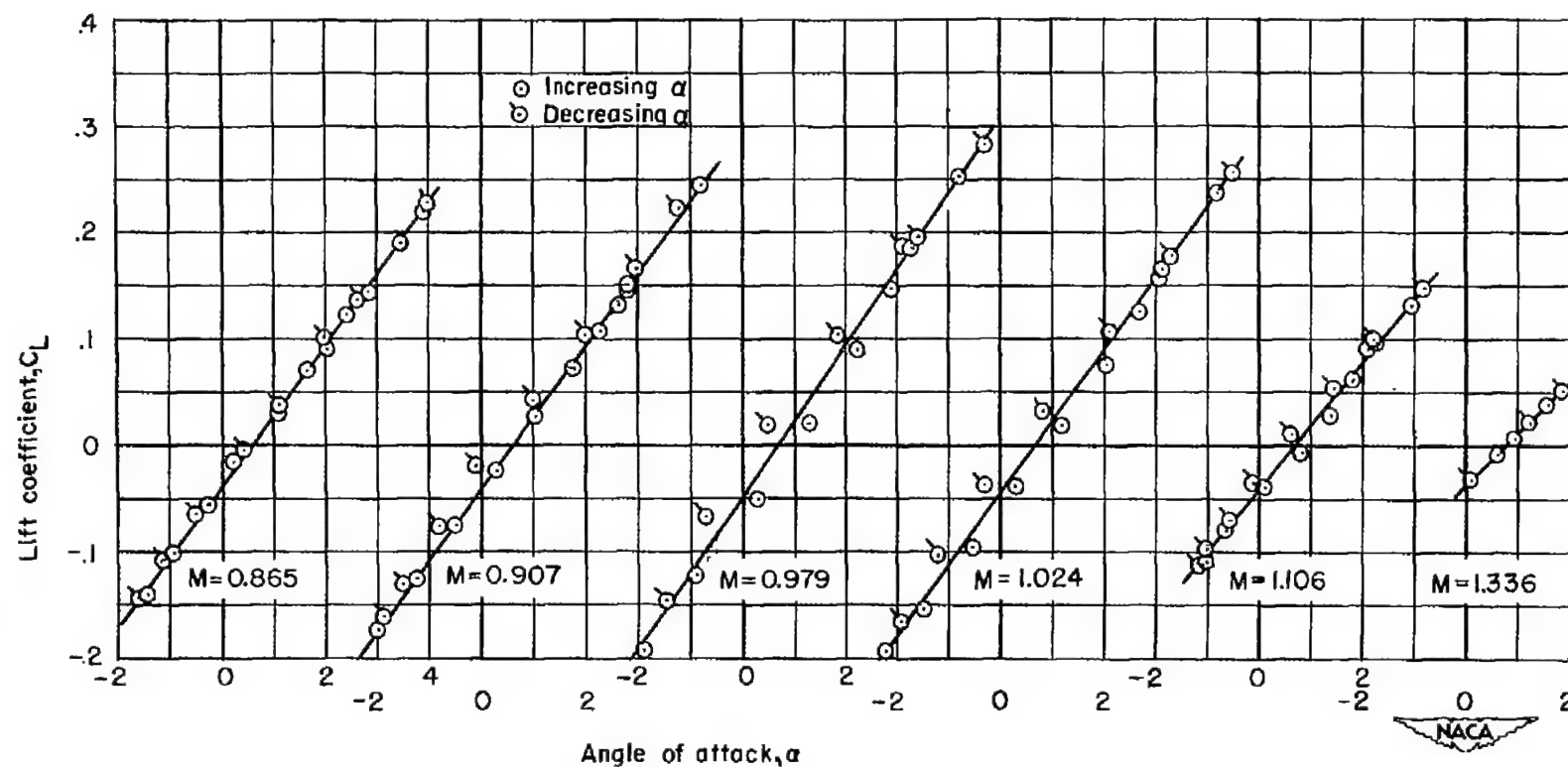
(a) Dural wing model.

Figure 6.- Variation of angle of attack with lift coefficient at various Mach numbers.
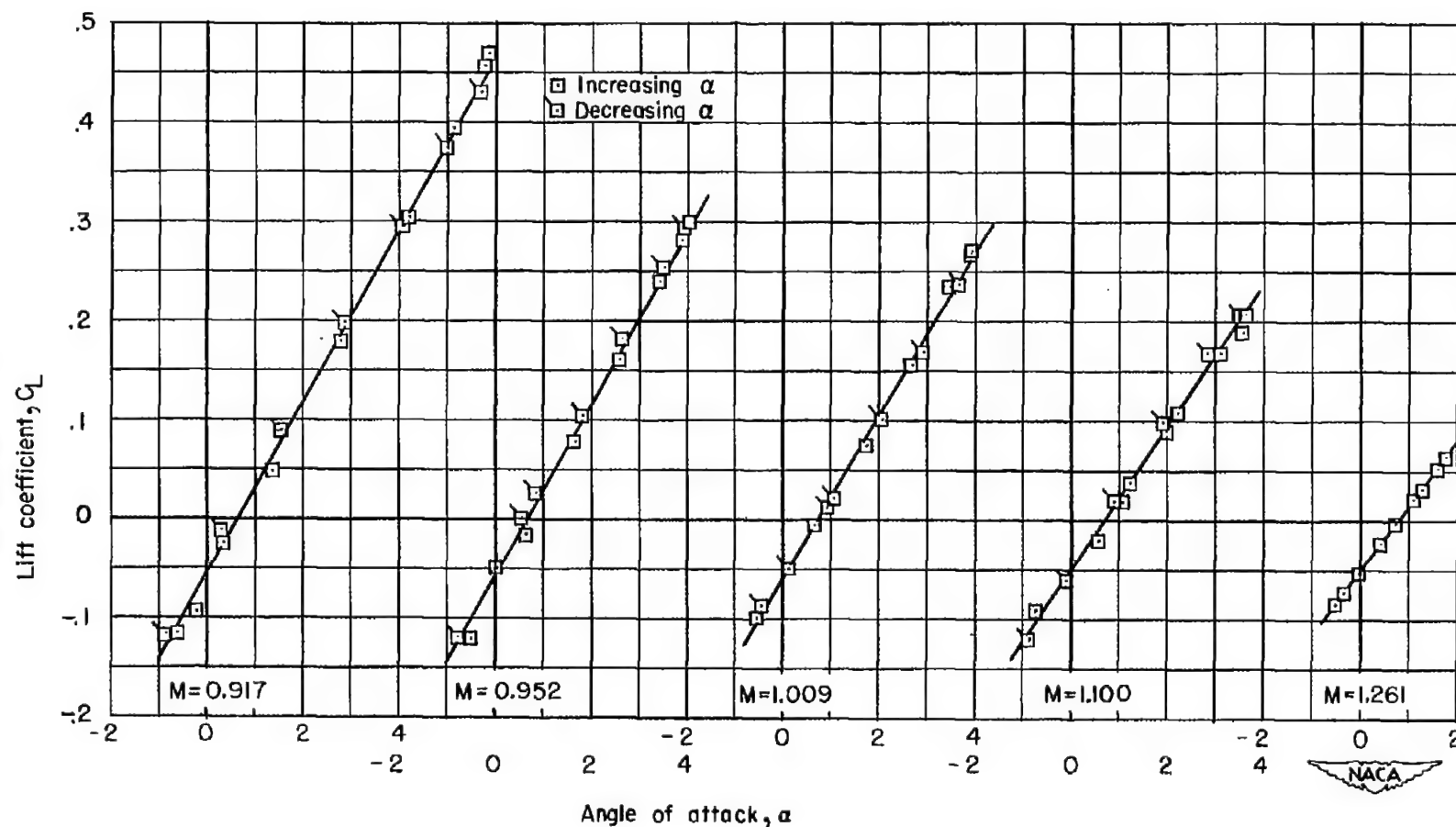
(b) Steel wing model.

Figure 6.- Concluded.
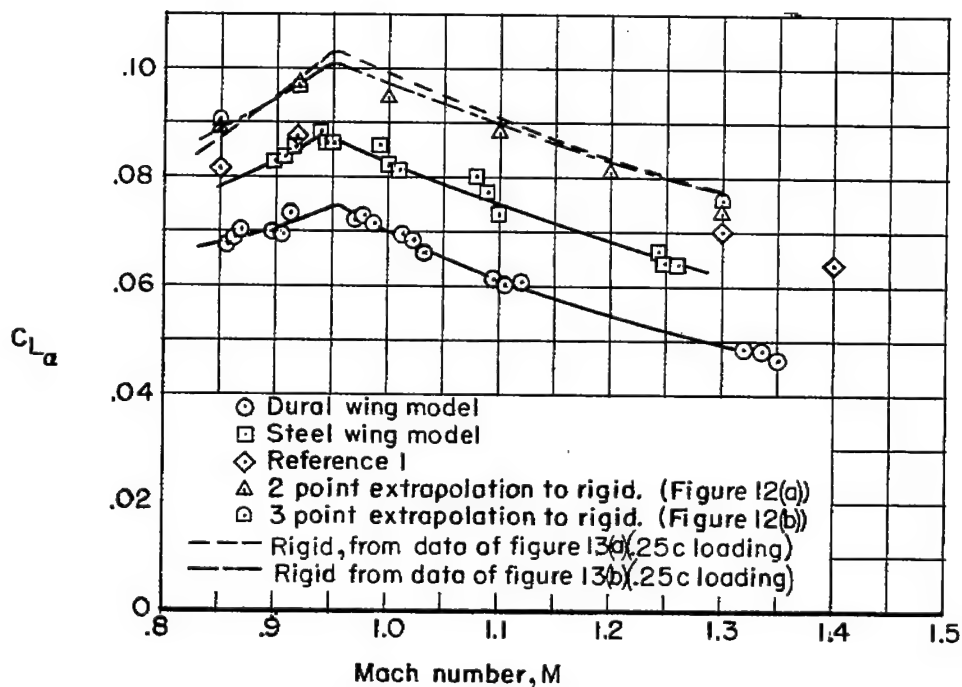
(a) Lift-curve slope.
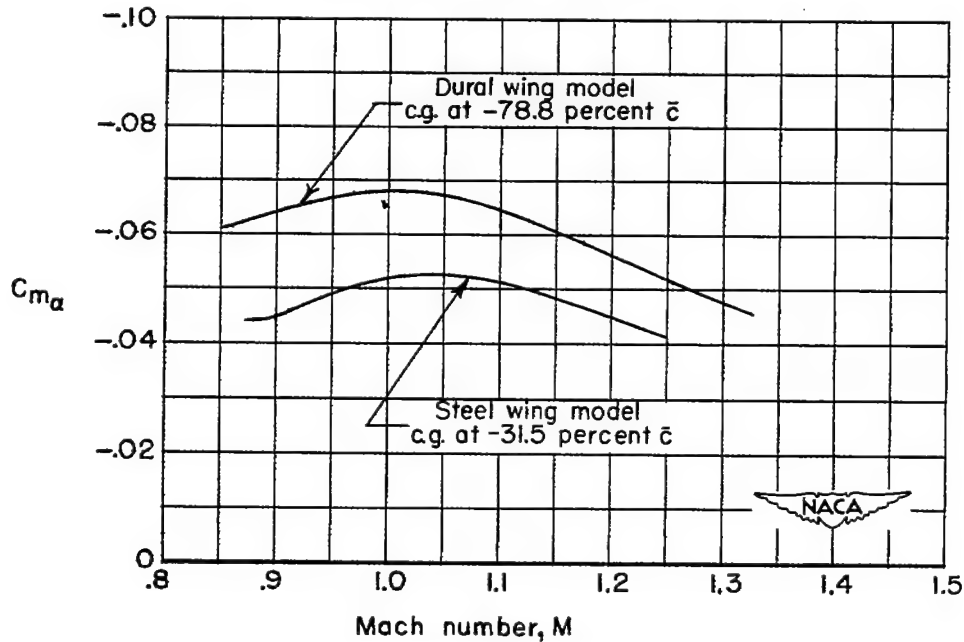
(b) Pitching-moment-curve slope.

Figure 7.- Effect of Mach number on the lift-curve and pitching-moment-curve slopes.
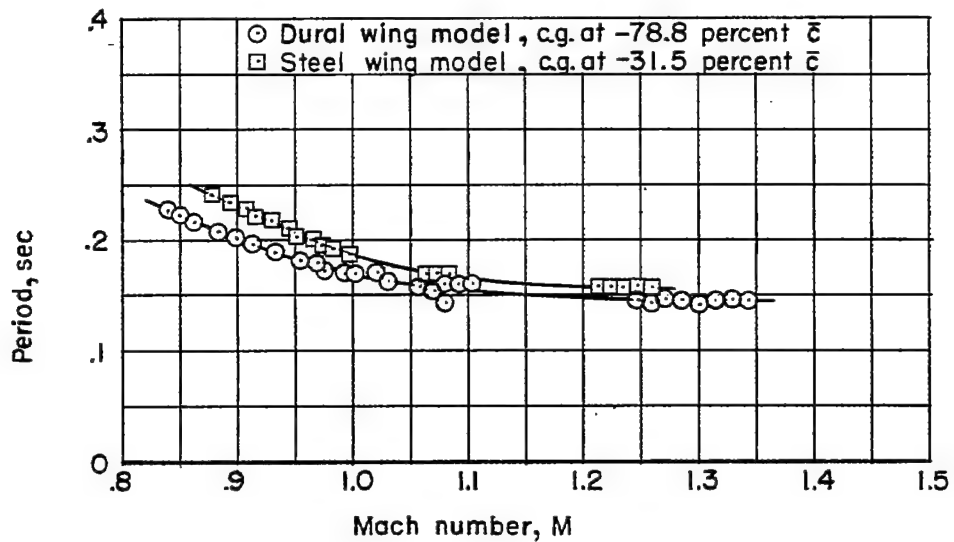
(a) Period of the longitudinal oscillation.
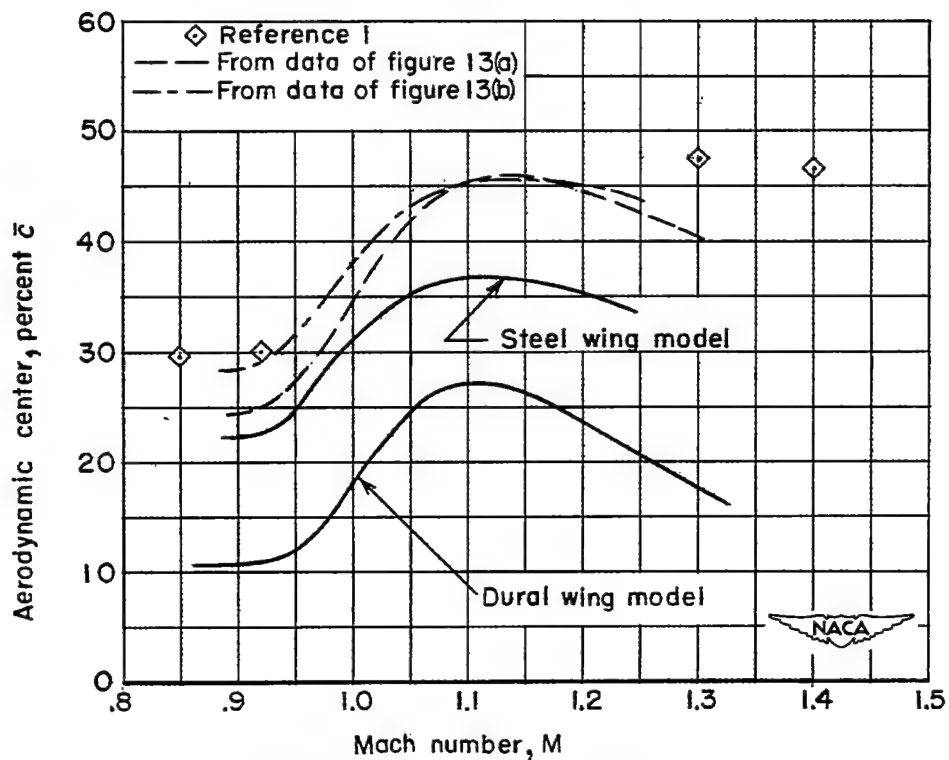
(b) Aerodynamic-center location.

Figure 8.- Period of the longitudinal oscillation and aerodynamic-center
location.

CONFIDENTIAL NACA RM L53F18
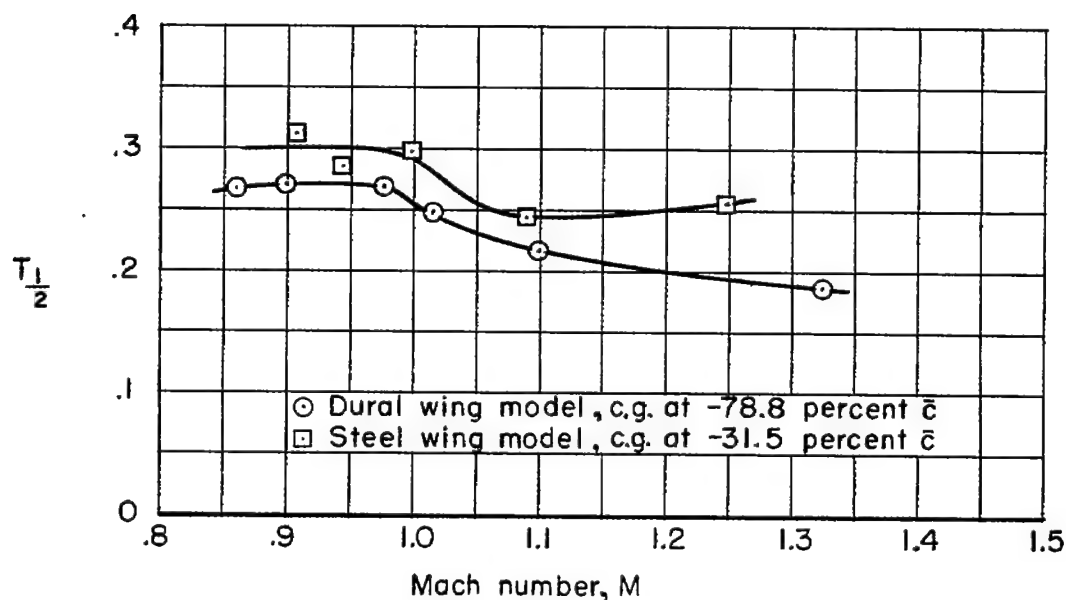
(a) Time to damp to one-half amplitude.
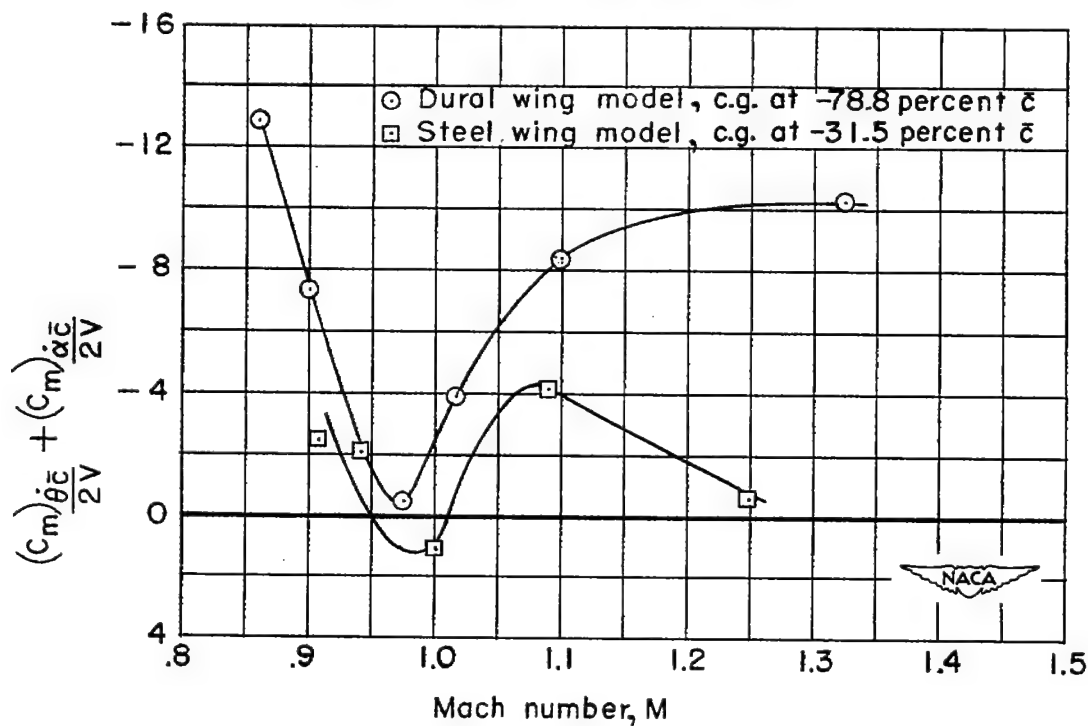
(b) Pitch-damping derivatives.

Figure 9.- Damping characteristics of the short-period longitudinal oscillation.

(a) Period of the lateral oscillation.
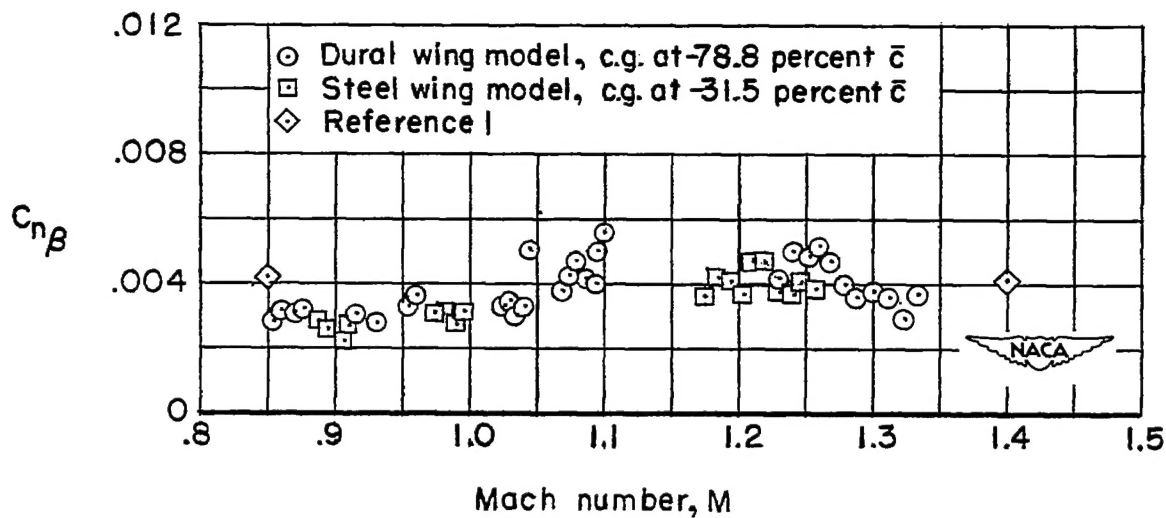
(b) Yawing-moment-curve slope.
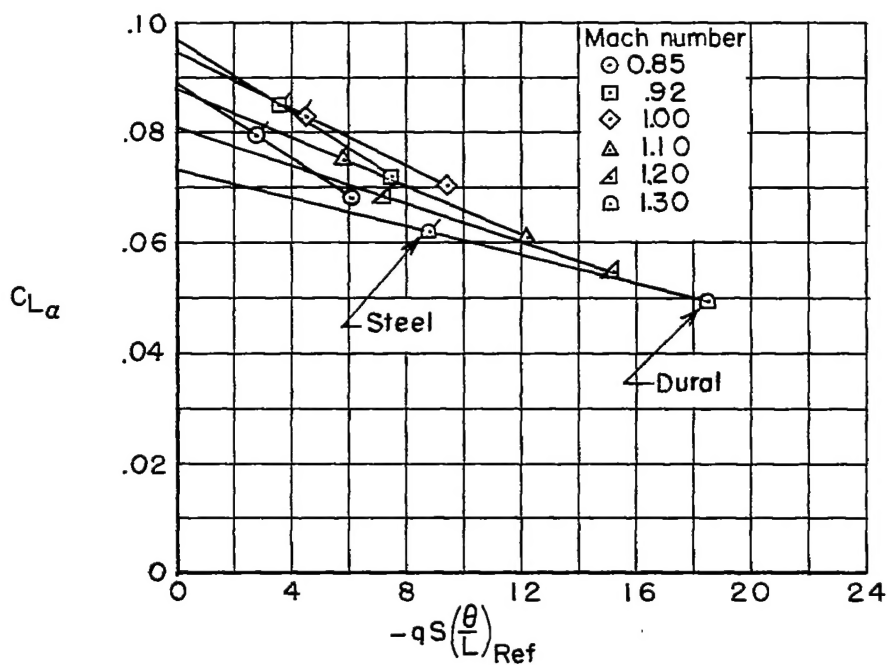
Figure 10.- Characteristics of the lateral oscillation.

CONFIDENTIAL
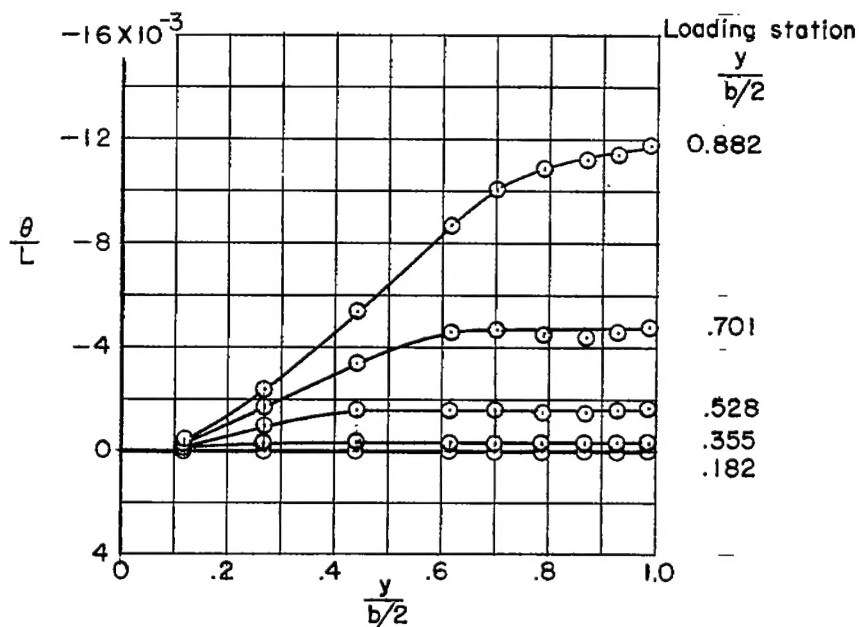
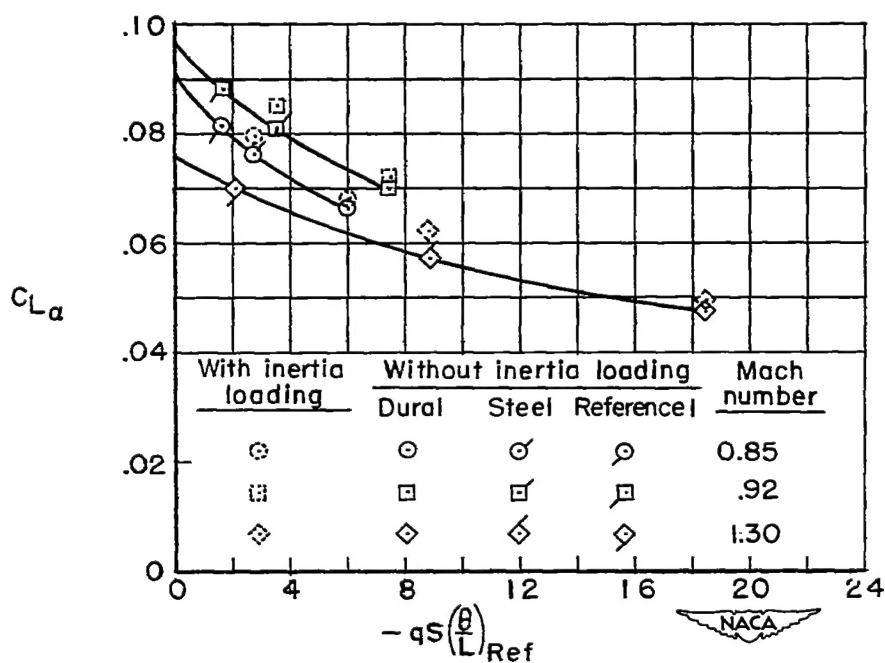(a) Loads applied along the 25-percent-chord line.
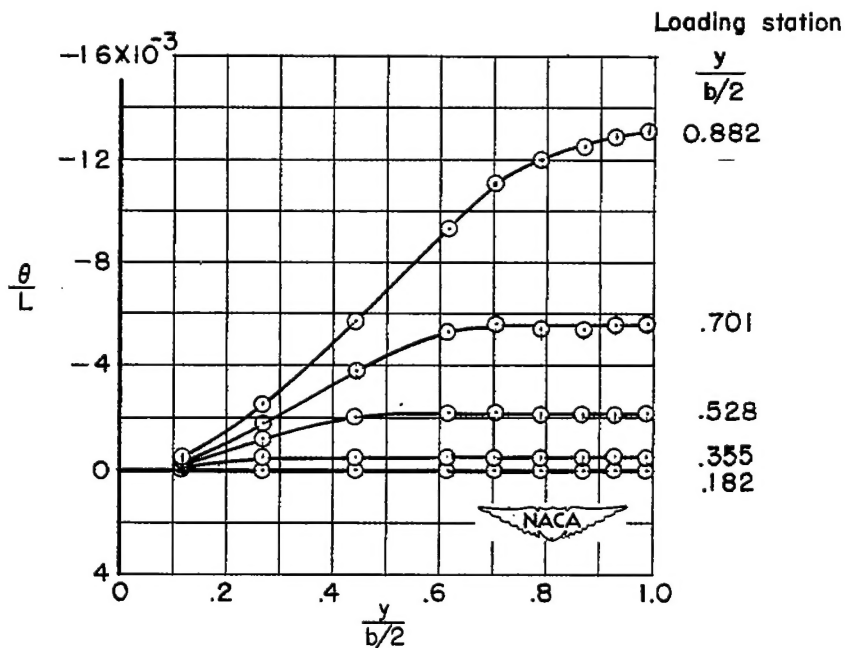
(b) Loads applied along the 40-percent-chord line.

Figure 11.- Streamwise angle of twist of the steel wing due to a unit
load applied along the 25- and 40-percent-streamwise-chord lines and
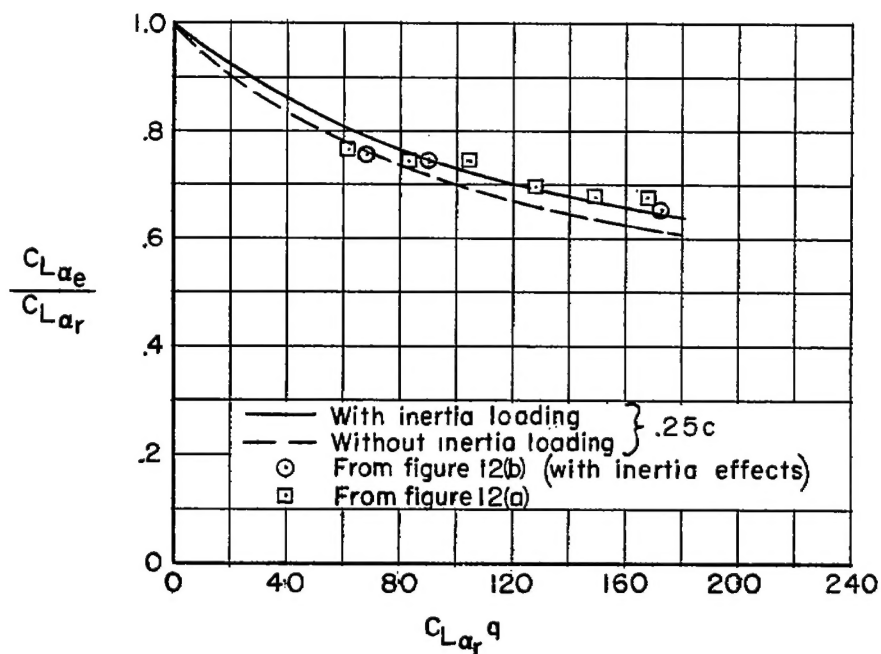at the spanwise stations indicated.
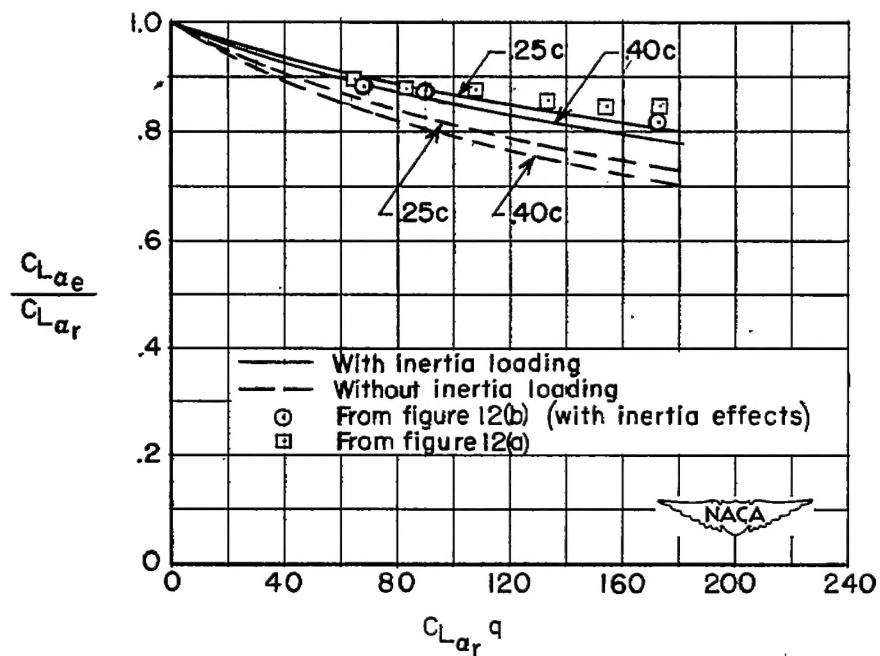
CONFIDENTIAL

(a) Two-point extrapolation.

(b) Three-point extrapolation.

Figure 12.- Two- and three-point extrapolation of experimental lift-curve
slopes to obtain rigid-wing lift-curve slopes.

CONFIDENTIAL

(a) Dural wing model.

(b) Steel wing model.

Figure 13.- Calculated and experimental ratio of elastic to rigid lift-curve slope for the dural and steel wing models.